Nanoscale Optical Biosensor: Short Range Distance Dependence of the Localized Surface Plasmon Resonance of Noble Metal Nanoparticles

Amanda J. Haes, Shengli Zou, George C. Schatz,* and Richard P. Van Duyne*

Department of Chemistry, Northwestern University, Evanston, Illinois 60208-3113

Received: August 1, 2003; In Final Form: March 19, 2004

Silver and gold nanotriangles were fabricated by nanosphere lithography (NSL) and their localized surface plasmon resonance (LSPR) spectra were measured by UV−vis extinction spectroscopy. It is demonstrated that the short range (viz., 0−2 nm) distance dependence of the electromagnetic fields that surround these nanoparticles when resonantly excited can be systematically tuned by changing their size, structure, and composition. This is accomplished by measuring the shift in the peak wavelength, λ_{max}, of their LSPR spectra caused by the adsorption of hexadecanethiol as a function of nanoparticle size (in-plane width, out-of-plane height, and aspect ratio), shape (truncated tetrahedron versus hemisphere), and composition (silver versus gold). We find that the hexadecanethiol-induced LSPR shift for Ag triangles decreases when in-plane width is increased at fixed out-of-plane height or when height is increased at fixed width. These trends are the opposite to what was seen in an earlier study of the long range distance dependence in which 30 nm thick layers were examined (Haes et al. *J. Phys. Chem. B* **2004**, *108*, 109), but both the long and short range results are confirmed by a theoretical analysis based on finite element electrodynamics. The theory results also indicate that the short range results are primarily sensitive to hot spots (regions of high induced electric field) near the tips of the triangles, so this provides an example where enhanced local fields play an important role in extinction spectra. Our measurements further show that the hexadecanethiol-induced LSPR peak shift is larger for nanotriangles than for hemispheres with equal volumes and is larger for Ag nanotriangles than for Au nanotriangles with the same in-plane widths and out-of-plane heights. The dependence of the alkanethiol-induced LSPR peak shift on chain length for Ag nanotriangles is approximately size-independent. We anticipate that the improved understanding of the short range dependence of the adsorbate-induced LSPR peak shift on nanoparticle structure and composition reported here will translate to significant improvements in the sensitivity of refractive-index-based nanoparticle nanosensors.

I. Introduction

The use of noble metal nanoparticles as nanoscale optical biosensors and chemosensors is beginning to receive significant attention.[2−32] This application arises from the unique nanoparticle optical properties of certain materials such as silver and gold. It is now well-established that optical excitation of the localized surface plasmon resonance (LSPR) of silver and gold nanoparticles results in absorption with extremely large molar extinction coefficients of $\sim 3 \times 10^{11}$ M^{-1} cm^{-1},[33−35] resonant Rayleigh scattering[3,36] with an efficiency equivalent to that of 10^6 fluorophors,[7,8] and strong enhancement of the local electromagnetic fields near the nanoparticle surface.[37,38] Furthermore, the peak extinction or resonant Rayleigh scattering wavelength, λ_{max}, intensity, and line width of these LSPR spectra are strongly dependent on their size, shape, interparticle spacing, and local dielectric environment.[16,33,34,38−45] Consequently, five different nanoparticle-based sensing mechanisms have been reported that enable the transduction of macromolecular or chemical binding events into optical signals. These mechanisms are (1) resonant Rayleigh scattering from nanoparticle labels in a manner analogous to fluorescent dye labels,[2−9] (2) nanoparticle aggregation,[10−15] (3) charge-transfer interactions at nanoparticle surfaces,[16−21,32] (4) local refractive index changes,[18,22−29,32] and (5) surface-enhanced Raman scattering.[30]

Recently, it has been demonstrated that Ag nanotriangles fabricated by nanosphere lithography (NSL) function as extremely sensitive chemical and biological optical nanosensors by monitoring adsorption-induced shifts in the LSPR peak extinction.[18,27−29] NSL has been a nearly ideal nanofabrication tool for these studies since it can produce surface-confined nanoparticles with fixed interparticle spacings in a massively parallel manner. As a consequence, NSL-derived nanoparticles do not aggregate and behave optically as *N* weakly coupled nanoparticles rather than as an array of strongly coupled nanoparticles. Thus NSL-derived nanoparticles permit us to focus on sensing mechanisms involving local refractive index changes and/or charge-transfer interactions independent of aggregation mediated optical responses. Furthermore, NSL allows for the easy manipulation of the nanoparticle size, shape, and composition.[39,46]

In previous work, Van Duyne and co-workers measured the distance dependence of the LSPR extinction maximum of Ag nanoparticles (in-plane width $a = 100$ nm, out-of-plane height $b = 50$ nm) synthesized by NSL via three pathways. First, systematic studies demonstrated that the LSPR λ_{max} extinction maximum of triangular Ag nanoparticles was so sensitive to the presence of alkanethiol adsorbates that it exhibited a linear red-shift corresponding to 3.3 nm for every carbon atom in the alkane chain accompanied by an 8.5 nm blue-shift due to the Ag−S charge-transfer interaction.[18] As an additional proof of concept, it was shown that the LSPR λ_{max} reversibly red-shifted

* To whom correspondence may be addressed. E-mail: vanduyne@chem.northwestern.edu (R.P.V.D.); schatz@chem.northwestern.edu (G.C.S.).

10.1021/jp036261n CCC: $27.50
Published on Web 04/29/2004

by ~5 nm in response to the electrostatic adsorption of the polypeptide poly-L-lysine to Ag nanoparticles modified with deprotonated carboxylate groups from 11-mercaptoundecanoic acid (11-MUA). Finally, it was shown that LSPR nanosensor could be used to detect <1 pM streptavidin and <100 pM anti-biotin to biotinylated Ag nanoparticles with almost no nonspecific binding effects.[27,29]

In a recent study, we demonstrated that the sensitivity of nanoparticle-based sensors, in comparison to flat surface plasmon resonance (SPR) sensors, arises primarily due to relatively short (~30 nm) electromagnetic field decay length of the Ag nanoparticles.[1] This was done by using a layer-by-layer assembly technique to functionalize the nanoparticles with up to 30 nm of alkanethiols, thereby revealing the distance dependence of the nanoparticle optical response. In addition, we performed accurate electrodynamics simulations of these functionalized nanoparticles and demonstrated quantitative agreement with the measurements with respect to the distance dependence of the plasmon resonance wavelength shift. By combining experiment with theory, we also found that LSPR nanosensors possess at least two unique characteristics that can be tuned by changing the nanoparticles' size and shape. These are (1) modest refractive sensitivity on the order of 1 part in 10^2 and (2) a sensing length scale on the order of tens of nanometers that is determined by the characteristic decay length of the average electromagnetic field.

In this paper, we explore the "short"-range (viz., $0 < d < 2$ nm) distance dependence of the LSPR nanosensor, with the goal of following up a prediction of our earlier work,[1] which suggested that hot spots (regions of locally enhanced electromagnetic fields) near the nanoparticle surface primarily control the size of the shift of the plasmon resonance when a layer of molecules is adsorbed. This prediction is to be contrasted with the "long"-range (i.e., 30 nm) results just mentioned, which are only sensitive to the average electromagnetic field. Thus, we will want to determine if changes in the extinction maximum induced by varying the composition, shape, and size of nanoparticles are different for a thin molecular self-assembled monolayer (SAM) than for a thick layer. To do this study, we perform four types of experiments. First, the sensitivity of different-shaped Ag nanoparticles to hexadecanethiol will be compared. The LSPR shift will be shown to be amplified for nonhemispherical nanoparticles. Second, the composition of Ag and Au nanoparticles with identical sizes and shapes will be varied and their sensitivity to hexadecanethiol will be compared. Because of differences in the orientation and packing density of SAM molecules on the nanoparticles, Ag nanoparticles exhibit approximately 3.5 times increased sensitivity over the Au nanoparticles. Next, trends in the LSPR extinction peak shift induced by a monolayer of hexadecanethiol as a function of the in-plane width and out-of-plane height of the Ag nanoparticles will be determined. Finally, the short range distance dependence of Ag nanoparticles ($a = 100$ nm, $b = 50$ nm; and $a = 78$ nm, $b = 30$ nm) will be probed by use of varying alkanethiol chain lengths.

An important conclusion from these results is that the trends in peak shift versus nanoparticle height and/or width are reversed compared to the corresponding trends seen earlier[1] in the longer range (~30 nm) optical response. To understand this, we have performed a detailed theoretical analysis based on finite element computational electrodynamics. The computations reproduce the observed variation of peak shift with nanoparticle shape, as well as the opposite correlation of short and long range response. As suggested by our earlier work, we are able to interpret these results in terms of the contributions of electrodynamic hot spots on the nanoparticle surface and how they vary with nanoparticle shape and size. From this, we learn that the short range optical response is sensitive to adsorbates located in remarkably small regions of the surface that comprise only about 10% of the exposed surface area of the nanoparticle.

II. Experimental Section

Materials. 1-Propanethiol, 1-butanethiol, 1-pentanethiol, 1-hexanethiol, 1-heptanethiol, 1-octanethiol, 1-nonanethiol, 1-decanethiol, 1-dodecanethiol, hexadecanethiol, and octadecyl mercaptan were purchased from Aldrich (Milwaukee, WI). 1-Dodecanethiol and *n*-pentadecyl mercaptan were purchased from TCI (Portland, OR). 1-Tetradecanethiol was purchased from Fluka. Absolute ethanol was purchased from Pharmco (Brookfield, CT). Hexanes and methanol were purchased from Fisher Scientific (Pittsburgh, PA). Ag wire (99.99%, 0.5 mm diameter) and Au wire (99.9%, 0.025 mm diameter) was obtained from D. F. Goldsmith (Evanston, IL). Borosilicate glass substrates, No. 2 Fisherbrand 18 mm circle coverslips were purchased from Fisher Scientific (Pittsburgh, PA). Tungsten vapor deposition boats were acquired from R. D. Mathis (Long Beach, CA). Polystyrene nanospheres with diameters of 280 ± 4 nm, 310 ± 9 nm, 400 ± 8 nm, 450 ± 5 nm, and 510 ± 11 nm were received as a suspension in water (Interfacial Dynamics Corporation, Portland, OR) and were used without further treatment. Millipore cartridges (Marlborough, MA) were used to purify water to a resistivity of 18 MΩ. All materials were used without further purification.

Substrate Preparation. Glass substrates were cleaned in a piranha solution (1:3 30% H_2O_2/H_2SO_4) at 80 °C for 30 min. Once cooled, the glass substrates were rinsed with copious amounts of water and then sonicated for 60 min in 5:1:1 $H_2O/NH_4OH/30\%$ H_2O_2. Next, the glass was rinsed repeatedly with water and was stored in water until used.

Nanoparticle Preparation. NSL was used to fabricate monodisperse, surface-confined Ag and Au nanoparticles.[39,46] For these experiments, single-layer colloidal crystal nanosphere masks were prepared by drop coating ~2 μL of nanosphere solution onto glass substrates. Once the nanosphere masks were dry, the substrates were mounted into a Consolidated Vacuum Corp. vapor deposition system. A Leybold Inficon XTM/2 quartz crystal microbalance (East Syracuse, NY) was used to measure the thickness of the Ag or Au film deposited over the nanosphere mask. The in-plane width (or perpendicular bisector) of the nanoparticles was varied by changing the nanosphere diameter used in the NSL process. Depositing controlled amounts of metal onto the nanosphere mask varied the out-of-plane height of the nanoparticles. Following metal deposition, the nanosphere mask was removed by sonicating the sample in ethanol for 3 min. The samples were either thermally annealed for 1 h at ~600 °C in the aforementioned thermal or solvent annealed. Finally, the samples were dosed with 1 mM alkanethiol solutions (in ethanol) for 18−24 h. The self-assembled monolayer (SAM) functionalized nanoparticles were then rinsed thoroughly to remove all physisorbed molecules. The topic of nanoparticle adhesion has been addressed in previous work.[29] Ag adhesion to glass substrates is poor; however, in the absence of aqueous solutions, nanoparticle adhesion is sufficient. Because all assays presented here are performed in an ethanolic environment, the adhesion between the glass substrates and the nanoparticles is adequate.

Nanoparticle Solvent Annealing. A home-built flow cell[18] was used to control the external environment of the Ag

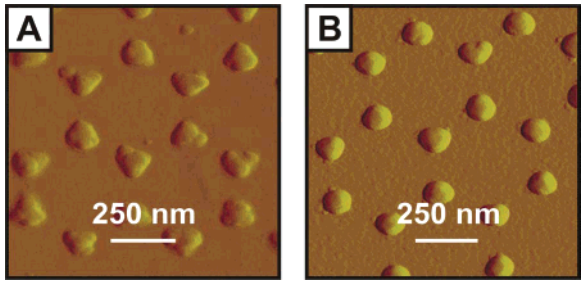

Figure 1. Representative tapping-mode AFM images of Ag nanoparticles (nanosphere diameter, $D = 400$ nm, $d_m = 50.0$ nm). Scan areas $\sim 1\ \mu m^2$. Scan rate = 2.0 Hz. (A) After solvent annealing, the resulting nanoparticles have in-plane widths $a = 114$ nm and out-of-plane widths $b = 54$ nm. (B) After thermal annealing of the sample at 650 °C for 1 h, the resulting nanoparticles have in-plane widths of ~110 nm and out-of-plane heights of ~61 nm.

nanoparticle substrates. Prior to modification, the Ag nanoparticles were solvent annealed[18] with hexanes and methanol. Dry N_2 gas and solvent were cycled through the flow cell until the λ_{max} of the sample stabilized. Samples were then incubated in 1 mM SAM ethanolic solutions for 24 h. After incubation, the nanoparticle samples were rinsed with ethanol and dried by flowing N_2 gas through the sample cell.

Ultraviolet−Visible Extinction Spectroscopy. Macroscale UV−vis extinction measurements were collected using an Ocean Optics (Dunedin, FL) SD2000 fiber optically coupled spectrometer with a CCD detector. All spectra collected are macroscopic measurements performed in standard transmission geometry with unpolarized light. The probe beam diameter was approximately 2 mm.

Atomic Force Microscopy. AFM images were collected using a Digital Instruments Nanoscope IV microscope and a Nanoscope IIIA controller operating in tapping mode. Etched Si nanoprobe tips (TESP, Digital Instruments, Santa Barbara, CA) were used. These tips had resonance frequencies between 280 and 320 kHz and are conical in shape with a cone angle of 20° and an effective radius of curvature at the tip of 10 nm. All images shown here are unfiltered data that were collected in ambient conditions. The height of the nanoparticle, *b*, was determined by AFM.

III. Results and Discussion

Nanoparticle Shape Dependence of Adsorbate- (Hexadecanethiol-) Induced LSPR Shifts. NSL was used to synthesize Ag nanoparticles on glass substrates. A representative AFM image of solvent-annealed Ag nanoparticles is found in Figure 1A. The nanoparticles have approximate in-plane widths (*a*) of 114 nm, out-of-plane heights (*b*) of 54 nm, and a truncated tetrahedral (triangular) shape. After thermal annealing the nanoparticle sample in a 1×10^{-6} Torr environment at 650 °C for 1 h, the triangular nanoparticles (Figure 1A) are converted into hemispherical nanoparticles with in-plane widths of 110 nm and out-of-plane heights of 61 nm (Figure 1B).

The corresponding UV−vis extinction spectra of the aforementioned samples can be found in Figure 2 (spectrum 1 in each panel). The LSPR extinction maximum, λ_{max}, of the hemispherical nanoparticle sample is blue-shifted by ~150 nm from the λ_{max} of the chopped tetrahedral nanoparticle sample. This trend consistent with the results of electrodynamic theory,[35,47,48] and it arises both from the less oblate structure and from the absence of sharp points on the annealed nanoparticle.

After incubation in 1 mM hexadecanethiol, the λ_{max} of the triangular nanoparticles shifted from 594.8 nm (spectrum 1, Figure 2A) to 634.8 nm (spectrum 2, Figure 2

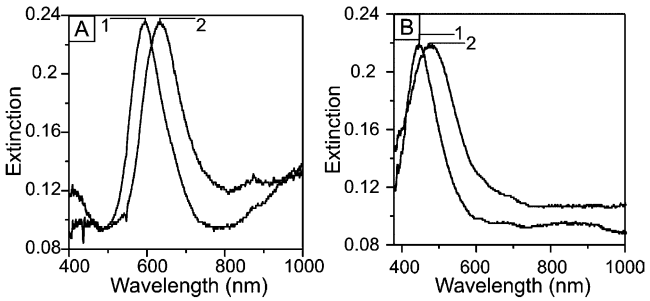

Figure 2. LSPR spectra of nanoparticles ($a = 100$ nm, $b = 50.0$ nm) in a N_2 environment. (A) Ag nanoparticles (1) before chemical modification, $\lambda_{max} = 594.8$ nm, and (2) after modification with 1 mM hexadecanethiol, $\lambda_{max} = 634.8$ nm. (B) Annealed Ag nanoparticles (1) before chemical modification, $\lambda_{max} = 438.8$ nm, and (2) after modification with 1 mM hexadecanethiol, $\lambda_{max} = 466.4$ nm.

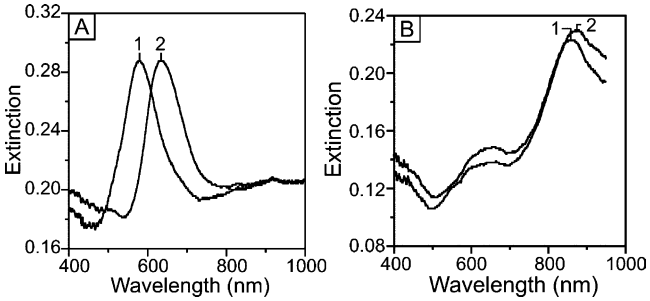

Figure 3. LSPR spectra of nanoparticles ($a = 100$ nm, $b = 75.1$ nm) in a N_2 environment. (A) Ag nanoparticles (1) before chemical modification, $\lambda_{max} = 563.0$ nm, and (2) after modification with 1 mM hexadecanethiol, $\lambda_{max} = 611.1$ nm. (B) Au nanoparticles (1) before chemical modification, $\lambda_{max} = 860.7$ nm, and (2) after modification with 1 mM hexadecanethiol, $\lambda_{max} = 874.5$ nm.

A). This 40.0 nm red-shift can be attributed to the 2.61 nm thick adsorbate layer in the nanoparticles' local dielectric environment.[49] The hemispherical nanoparticle sample exhibits a smaller extinction shift upon exposure to hexadecanethiol in comparison to the truncated tetrahedral nanoparticles. For the hemispherical nanoparticle sample, the λ_{max} shifts from 438.8 nm (spectrum 1, Figure 2B) to 466.4 nm (spectrum 2, Figure 2B), resulting in a 27.6 nm LSPR shift. This smaller peak shift is the same as was found in our earlier studies of the longer range (~30 nm) response.[1] In that work, an electrodynamics study demonstrated that the more red-shifted plasmon resonances gave larger peak shifts.

Nanoparticle Composition Dependence of Adsorbate-(Hexadecanethiol-) Induced LSPR Shifts. Because NSL is a materials-flexible technique, a comparison of how the composition of the nanoparticles with identical sizes and shapes influences the LSPR extinction shift for hexadecanethiol is studied. Figure 3A, spectrum 1 is the LSPR spectrum of truncated tetrahedral nanoparticles with in-plane widths of 100 nm and out-of-plane heights of 75.1 nm. After exposure to hexadecanethiol, the extinction maximum shifts from 563.0 to 611.1 nm (Figure 3A, spectrum 2). The LSPR spectrum of Au nanoparticles with identical sizes and shapes (as the previous Ag sample) is shown in Figure 3B, spectrum 1. Dipole and quadrupole peaks are located at 860.7 and 659.1 nm, respectively.[50] Upon exposure to hexadecanethiol, the dipole peak shifts to 874.5 nm while the quadrupole peak remains relatively constant at 659.5 nm (Figure 3B, spectrum 2).

Figure 3 shows that the Ag sample has a much larger LSPR shift than the Au sample (38.1 vs 13.8 nm). Although a portion of this difference can be attributed to varying electromagnetic field strengths surrounding the nanoparticles, the dominant

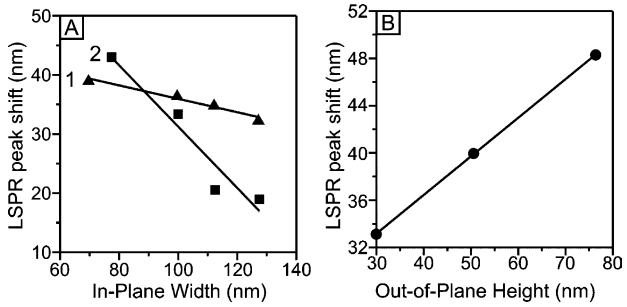

Figure 4. Hexadecanethiol LSPR shift dependence on Ag nanoparticle size. (A) (1) Ag nanoparticles with a fixed out-of-plane height, $b = 50.0$ nm, and varying in-plane width. Linear regression was used to fit the data to a line described by $y = -0.1135x + 47.3$. (2) Ag nanoparticles with a fixed out-of-plane height, $b = 30.0$ nm, and varying in-plane width. Linear regression was used to fit the data to a line described by $y = -0.52x + 83.5$. (B) Ag nanoparticles with a fixed in-plane width, $a = 100$ nm, and varying out-of-plane height. Linear regression was used to fit the data to a line described by $y = 0.33x + 23.6$.

difference between the two samples is the SAM packing density,[51] tilt angle, and resulting SAM thickness[49,52] on Au versus Ag. The SAM layer thickness of hexadecanethiol on Ag is ~2.61 nm,[49] while on Au it is ~2.16 nm.[52] Because the overall nanoparticle response is sensitive to layer thickness, the LSPR shift for hexadecanethiol on Au should be less than the LSPR shift for Ag nanoparticles.

Nanoparticle Size/Shape Dependence of Adsorbate- (Hexadecanethiol) Induced LSPR Shifts. Because the height and width of NSL-derived nanoparticles can be varied by changing the deposition thickness (d_m) and nanosphere diameter (D), respectively; the relationship between the LSPR peak shift versus in-plane width and out-of-plane height can easily be monitored. Clear trends are displayed for fixed nanoparticle height. Figure 4A, line 1 displays the LSPR shift for Ag nanoparticles with a fixed out-of-plane height of 50.0 nm and varying in-plane widths. It was found that, for every 10 nm increase in the width of the nanoparticles, the LSPR shift decreased by ~1.1 nm. A similar experiment was performed on 30.0 nm tall Ag nanoparticles (Figure 4A line 2). It was found that, for every 10 nm increase in the in-plane width of the nanoparticles, the LSPR shift decreased by ~5.2 nm. The LSPR shift for hexadecanethiol for Ag nanoparticles with fixed in-plane width and varying out-of-plane height is shown in Figure 4B. It was found that as the out-of-plane height increased by 10 nm, the LSPR shifts increase by ~3.3 nm. The trends for all three plots follow aspect ratio arguments. That is, as the aspect ratios of the nanoparticles increase, the LSPR peak shifts decrease. Additionally, no clear trends exist for LSPR shifts versus surface area or volume (data not shown).

Chain Length Dependence of LSPR Shift for Ag Nanoparticles. It was shown in an earlier publication that the LSPR extinction wavelength of NSL-derived triangular nanoparticles shifts by 3.3 nm for every carbon atom in an adsorbed $CH_3(CH_3)_xSH$ monolayer for $x = 3, 5, 7, 9, 11, 13$, and 15.[18] Figure 5 expands that data set by including SAM layers where $x = 2-11$, 13−15, and 17). To analyze these results the data were first treated by considering even or odd number of carbons in the alkanethiol chain lengths. Previous studies with contact angle measurements and external reflection infrared spectroscopy have indicated slight orientation differences between odd- and even-length alkanethiol molecules on gold and silver, so we determined whether this made a difference in our results. For nanoparticles with in-plane widths of 100 nm and out-of-plane heights of 50.0 nm Ag, the slopes of the best-fit line that

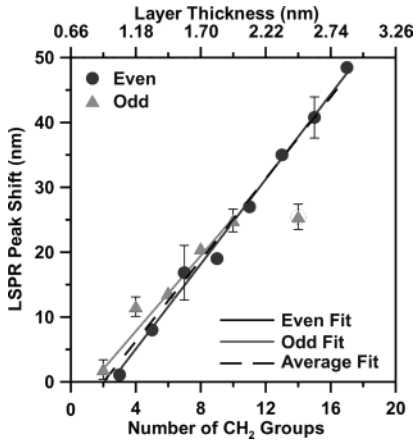

Figure 5. Even and odd alkanethiol chain length and layer thickness dependence on the LSPR spectral peak shifts for Ag nanoparticles with $a = 100$ nm, $b = 50.0$ nm. All extinction measurements were collected in a N_2 environment. Data points represent the averaged results. Error bars show the variation in the raw data. Linear regression was used to fit even, odd, and all data. The even data can be fit to a line described by $y = 3.3x - 8.0$. The odd data can be fit to a line described by $y = 2.9x - 4.0$. The entire data set can be fit to a line described by $y = 3.1x - 6.3$. The circled outlying data point was not used when the data were fitted.

describes the data are 3.3 and 2.9 nm LSPR shift per CH_2 group in the alkanethiol even and odd chain lengths, respectively. Although these values differ slightly, considering packing efficiencies for long (≥9 CH_2 groups) versus short (<8 CH_2 groups) and considering that the majority of the odd lengths contain <8 CH_2 groups, this difference is not sufficient to support or refute packing differences between the two data sets. For that reason, a valid description of the data can be used by treating the entire data set. When doing this, the slope of the best-fit line that matches these data is refined to 3.1 nm LSPR shift per CH_2 group in the alkanethiol chain. Additionally, the y-intercept, which is related to the Ag−S charge-transfer interaction, is refined to −6.3 nm.

Because the theme of this paper is to understand how the short range distance dependence of the LSPR nanosensor changes as a function of nanoparticle size, shape, and composition, the previous experiment was repeated for Ag nanoparticles having $a = 73$ nm and $b = 30.0$ nm. It should be noted that the sample in Figure 6 has a higher aspect ratio and volume and gave a larger LSPR shift upon exposure to hexadecanethiol than Ag nanoparticles having $a = 100$ nm and $b = 50.0$ nm (Figure 5). The LSPR extinction wavelength shifts 3.1 nm per CH_2 group in the alkanethiol chain length (Figure 6). By fitting the data to a straight line, the Ag−S charge-transfer band is calculated to be −8.1 nm. On the basis of ellipsometry data by Porter et al.,[49] the layer thickness associated with each alkanethiol length can be estimated (as seen on the upper x axis of both Figures 5 and 6).

Comparing the data of Figures 5 and 6 reveals extremely similar results in the CH_2 group sensitivity and in the Ag−S charge interaction. While the two nanoparticle sizes exhibit different behaviors for hexadecanethiol exposure, it is suspected that their sizes do not vary by a large enough degree to result in varying behaviors for multiple alkanethiol SAM length studies.

Estimation of Refractive Index and Layer Thickness of a Hexadecanethiol Monolayer on Ag Nanoparticles. Ellipsometry is routinely used to estimate monolayer thicknesses and dielectric constants of molecules on surfaces.[53,54] A limitation of these results is that small uncertainties in monolayer thickness

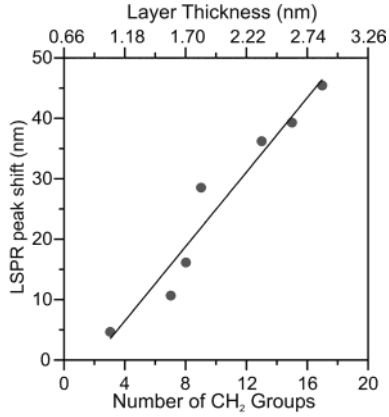

Figure 6. Alkanethiol chain length and layer thickness dependence on the LSPR spectral peak shifts for Ag nanoparticles with $a = 73$ nm, $b = 30.0$ nm. All extinction measurements were collected in a N_2 environment. Data points represent the averaged results. The variation of the data is contained within the data point size (therefore no error bars are included). Linear regression was used to fit the data to a line described by $y = 3.1x - 8.1$.

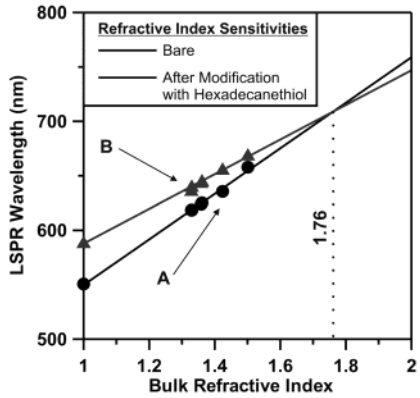

Figure 7. Bulk refractive index influences on bare and hexadecanethiol-modified nanoparticles. Extinction peak maxima of Ag nanoparticles ($a = 100$ nm, $b = 50$ nm) were measured in solvents with refractive indices ranging from 1.3288 (methanol) to 1.5011 (benzene). These data are representative of multiple experiments. (A) Unmodified nanoparticles. The data can be fit to a line described by $y = 209.0x + 340.8$. (B) Hexadecanethiol-modified nanoparticles. The data can be fit to a line described by $y = 159.1x + 428.8$. The point of intersection of these two lines, which corresponds to the approximate refractive index of the alkanethiol monolayer, is 1.76.

prevent this technique from accurately determining both of these parameters simultaneously. An alternative method that provides estimates of both average layer thickness and average dielectric constant is two-color surface plasmon resonance spectroscopy.[55] By using two different incident wavelengths for the surface plasmon resonance experiment and without changing other experimental parameters, properties of the monolayer are preserved, allowing for a more accurate estimation for both average monolayer thickness and average dielectric constant. It should be noted that the layer thicknesses used in this work are estimated by ellipsometry and AFM studies; therefore, the layer thicknesses noted are approximate and do not account for small packing efficiency differences that exist from sample to sample or from alkanethiol chain length variations.

In a two-color surface plasmon resonance experiment by Peterlinz and Georgiadis,[55] the refractive index of a hexadecanethiol monolayer on a gold thin film was determined to be ~1.46. If this value is used to predict wavelength shifts induced by alkanethiol layers on Ag nanoparticles, the magnitude of the LSPR shift is underestimated.[1] In an effort to understand this discrepancy, we performed a bulk refractive index sensitivity experiment in which the nanoparticle sample was exposed to solvents of varying refractive index before and after exposure to hexadecanethiol (Figure 7). The refractive index sensitivity of the Ag nanoparticles prior to hexadecanethiol modification is 196 nm/RIU. This value drops to 159 nm/RIU after functionalization in this molecule. As was shown previously,[18] the refractive index sensitivity of the nanoparticles to their bulk environment drops by ~20% following functionalization of the nanoparticles. By determining the intersection point between these two best-fit lines for the solvent sensitivities of the nanoparticle before and after functionalization, an estimate of the refractive index of the monolayer can be made. Surprisingly, in this case, the refractive index of the hexadecanethiol monolayer is estimated to be ~1.76. While this value is much larger than what is predicted by the two-color surface plasmon resonance experiment, it gives a result that is similar to the value (1.65) that we previously found matches the long range distance dependence of the LSPR peak shift. As a result, we will use the 1.65 value in the theoretical calculations that are presented below.

Theory. Previously, the long range (~30 nm)[1] effect on silver nanoparticle plasmon resonance peak shifts was modeled by use of a finite element electrodynamics method known as the discrete dipole approximation (DDA).[1,38,56] In this method, both the nanoparticle and the surrounding multilayer dielectric are represented in terms of cubical elements, and the optical response to an applied plane wave field is used to calculate extinction cross sections. Excellent agreement with the experimental results for the long range shift was obtained, with the only adjustable parameter in the calculation being the index of refraction of the molecular layer. As mentioned previously, a value of 1.65 was found to give the best fit. These calculations demonstrated that when the nanoparticle becomes more oblate, the LSPR of the bare nanoparticles red-shifts and the saturation shift induced by the adsorbate increases. Here, we have calculated the short range LSPR shift using the same approach and the same silver dielectric constant (taken from an experimental compilation from Lynch and Hunter)[57] and SAM index of refraction. In this treatment the dielectric constant is taken to be a local function, as there is no capability for a nonlocal description within the DDA approach. In addition to the closely related theoretical studies in ref 1, there have been several earlier studies in which the DDA method has been calibrated by comparison with experiment for truncated tetrahedral particles, including studies of external dielectric effects and substrate effects,[37,44,47] and on the basis of this, we expect DDA analysis to provide a useful qualitative description of the results.

The short range calculation is more difficult than the long range one because the grid size used in the DDA cannot be smaller than 1 nm if the calculations are to be feasible. In the long range calculation, a grid size of 2 nm was used as there were over 15 molecular layers present and effects of coarse graining on the extinction spectrum were small. In the short range calculation, there are only a few layers when we use a 1 nm grid, so graininess is more important. To examine this, results for layer thicknesses of 2, 3, and 4 nm will be evaluated.

The calculated results for a nanoparticle with height 30 nm and widths 78, 100, 112, and 128 nm are shown in Figure 8. Layer thicknesses of 2, 3, and 4 nm were considered. In contrast to the experimental results that show a decrease of the LSPR peak shift with increasing in-plane width, Figure 8 shows that the LSPR peak shift increases with increasing width. There is a decrease of the LSPR shift with the increasing width only

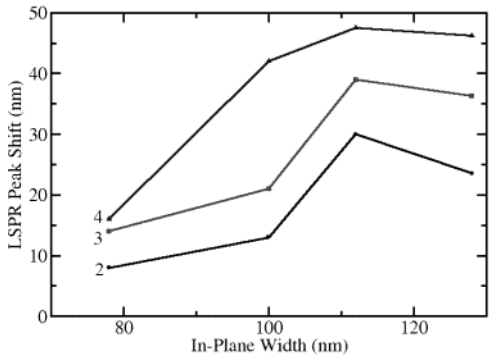

Figure 8. Plasmon wavelength shift versus in-plane nanoparticle size based on DDA calculations with layer dielectric constant of 1.65. Layer thicknesses of 2, 3, and 4 nm were considered.

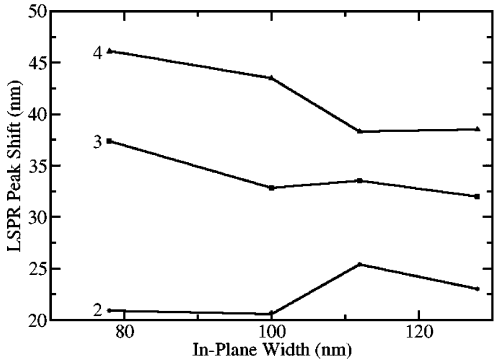

Figure 9. Plasmon wavelength shift versus in-plane nanoparticle size based on DDA calculations with layer dielectric constant of 1.65 and surrounded by an effective medium that describes the substrate interaction. Layer thicknesses of 2, 3, and 4 nm were considered.

when the width changes from 112 to 128 nm. One possible reason for the difference between theory and experiment is that the calculations were carried out with no substrate while the experiment is done with the nanoparticle on a substrate. This causes the LSPR peaks for bare nanoparticles to be blue-shifted relative to the experimental results, but its effect on the peak shift is hard to estimate without explicit calculations.

To study the effect of including the substrate, we have used the effective medium approximation of Kelly et al.[38] In this method, the effective dielectric constant of the medium that surrounds the nanoparticle and overlayer is defined as the weighted average of the dielectric constants of the substrate and of the vacuum above the molecular layer, with the weight determined by the relative areas of the nanoparticle and overlayer that are exposed to substrate and to vacuum. This approach was tested in earlier studies in which the substrate was explicitly included, and it was found to provide a realistic description of the extinction spectrum of a sphere that was partially sunk into the substrate at a small fraction of the computational effort of the explicit calculation. In the present application, this concept leads to the use a different effective dielectric constant for each nanoparticle structure, as the relative amounts of the nanoparticle that are exposed to the substrate change with structure. In particular, if the nanoparticle height is fixed and the width is increased, the contribution of the substrate becomes more important, and since the substrate index of refraction (taken to be 1.52) is larger than vacuum, this increases the effective dielectric constant.

The LSPR peak shifts based on the effective medium calculations are plotted in Figure 9. The calculated results for layer thicknesses of 3 and 4 nm show negative slopes that qualitatively agree with the experimental results. The 2 nm

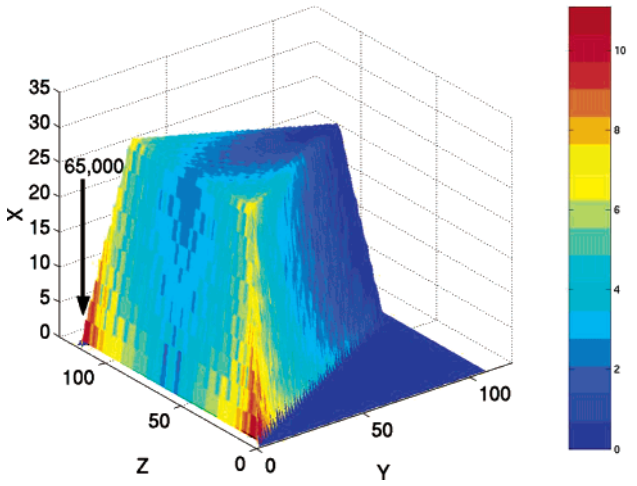

Figure 10. Local E-field (plotted as contours of log $|\mathbf{E}|^2$) for a Ag nanoparticle (a = 100 nm, b = 30 nm).

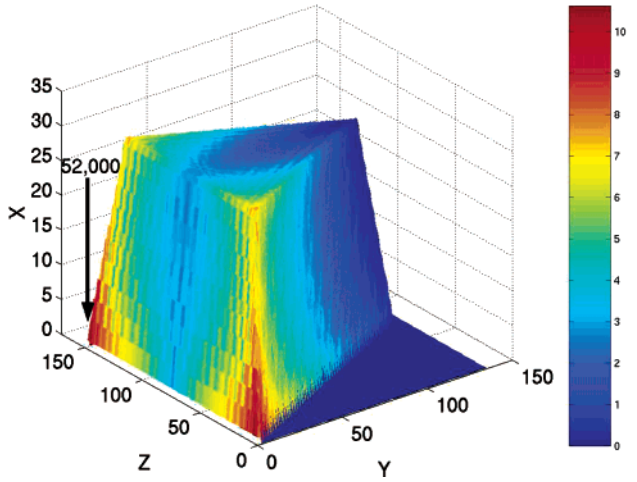

Figure 11. Local E-field (plotted as contours of log $|\mathbf{E}|^2$) for a Ag nanoparticle (a = 128 nm, b = 30 nm).

results are less consistent (showing an oscillation as a function of nanoparticle width), which likely is an indication of the influence of graininess in our model. For the 3 and 4 nm results, the reduction in peak shift over the 50 nm range of widths plotted is about 10 nm, so the slope (2 nm per 10 nm width change for the 30 nm height nanoparticle) is between the two experimental values determined earlier (1.1 nm per 10 nm width change for the 50 nm nanoparticle and 5.2 nm per 10 nm width change for the 30 nm nanoparticle). Given the crude nature of the effective medium model, as well as errors due to graininess and in the structural model of the adsorbed layer, the agreement is encouraging.

Now let us use the theoretical calculations to determine why the slopes in Figures 4 and 9 are negative while the corresponding slopes for the long range peak shift (determined in ref 1) are positive. We note first that, in our earlier work, we demonstrated that the long range peak shift is quantitatively determined by the behavior of the average local electric field as a function of the distance from the nanoparticle surface. In addition, we found that the field drops off more quickly with distance from the nanoparticle surface around hot spots than around cool spots, so the average behavior was more sensitive to hot spots for small distances from the surface (few nanometers) and to cool spots for larger distances (several tens of nanometers). To further explore this behavior, in Figures 10 and 11 we show contours of the logarithm of $|\mathbf{E}|^2$ for

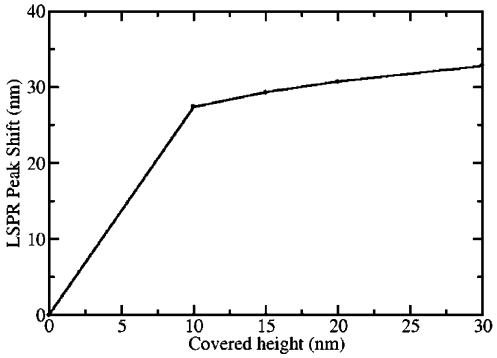

Figure 12. Plasmon peak shift versus height of the molecular layer for a 100 nm nanoparticle width, 30 nm height, and 3 nm layer thickness.

nanoparticles having widths of 100 and 128 nm as derived from the effective medium calculations. These figures show hot spots near the sharp points and cool regions in the flat parts of the triangles, similar to what we found earlier.

To show how the hot spots influence the peak shift, we have carried out calculations in which the molecular layer (assumed to be 3 nm thick) is chosen to cover only the lower portion of the exposed surface of the 100 nm wide nanoparticle. Figure 12 shows the LSPR peak shift as a function of the height of the layer. The plot shows that even when the layer covers only the lowest 10 nm of the surface of the 30 nm high nanoparticle (and the top has no layer at all), the peak shift is almost the same (27 vs 32 nm) as the fully covered nanoparticle. For the 10 nm high layer, only about 25% of the nanoparticle is covered with molecules. In other calculations we have observed that similar peak shifts can be obtained with portions of this 10 nm layer removed such that only 10% of the nanoparticle is covered. Thus, only the hot spots contribute significantly to the peak shift.

A key new feature of the results in Figures 10 and 11 is that the peak field for the 128 nm nanoparticle is lower than that for the 100 nm nanoparticle ($|\mathbf{E}|^2 = 52\,000$ versus 65 000). This lowering of the peak field occurs even though the plasmon resonance of the 128 nm nanoparticle is red-shifted relative to that of the 100 nm nanoparticle. Given the previously established correspondence between size of the peak shift and size of $|\mathbf{E}|^2$, we see that the negative slope in Figure 9 (14% reduction in peak shift in going from 100 to 128 nm) is a direct consequence of the 20% reduction in the value of $|\mathbf{E}|^2$ in Figure 11 compared to Figure 10.

There are three factors that can contribute to the $|\mathbf{E}|^2$ results in Figures 10 and 11: (1) $|\mathbf{E}|^2$ should increase in the quasistatic limit as the nanoparticle width is increased due to red-shifting of the plasmon resonance as the nanoparticle becomes more oblate. (2) $|\mathbf{E}|^2$ should decrease in the full electrodynamic description due to increased radiative damping effects as the nanoparticle width (and therefore size) is increased. (3) $|\mathbf{E}|^2$ will further decrease due to substrate dielectric effects, as the substrate contribution to the effective medium dielectric constant increases for increasing width, and larger dielectric constants lead to smaller fields. Factors 1 and 2 can be separated from 3 by calculating $|\mathbf{E}|^2$ without including the effective medium approximation. When we do this, we find that the peak $|\mathbf{E}|^2$ is larger in the absence of substrate effects (81 000 compared to 65 000 for the 100 nm nanoparticle) and it has a smaller drop (15% from 81 000 to 69 000) when the width changes from 100 to 128 nm. This indicates that some of the reduction in $|\mathbf{E}|^2$ is due to radiative damping; however, we note from Figure 8 that the slope is mostly positive if the substrate is not included. Thus we conclude that both factors 2 and 3 contribute to the drop in Figure 9.

IV. Conclusions

In this paper we have examined the short range (~2 nm) distance dependence of the plasmon resonance wavelength with nanoparticle composition, shape, and size using five distinct measurements. First, we found that truncated tetrahedral Ag nanoparticles have a ~1.5 times larger plasmon resonance shift than do hemispherical nanoparticles with identical volumes. Second, for a given size and shape (truncated tetrahedron), alkanethiols on Ag nanoparticles produce a ~3.5 times larger LSPR shift than do Au nanoparticles. Third, for a fixed nanoparticle height, plasmon peak shifts decrease linearly with increasing nanoparticle width. Fourth, for a fixed nanoparticle width, the peak shifts increase linearly with increasing nanoparticle height. Finally, it was shown that by changing the nanoparticle size, the alkanethiol sensitivity for increasing chain length, the methylene group sensitivity, and the Ag−S interaction remain approximately constant.

Perhaps the most surprising of these results is the decrease in peak shift with increasing nanoparticle width, as this is the opposite dependence to what was seen for the long range (~30 nm) distance dependence (and the nanoparticle height dependence is also inversely correlated). To understand this effect we performed detailed electrodynamics studies, and we found the same behavior as in the experiments. For the long range distance dependence, we found earlier that the increase in peak shift with increasing nanoparticle width arises from the effect of red-shifting of the plasmon resonance on the average local field at 30 nm distance from the nanoparticle surface. For the short range behavior, it is the field associated with hot spots near the nanoparticle surface that determine the effect, and here we find that $|\mathbf{E}|^2$ decreases as nanoparticle width increases. The decrease arises from two effects: increased radiative damping as nanoparticle size is increased (which is an especially important effect for nanoparticles larger than 100 nm), and reduction of $|\mathbf{E}|^2$ due to increased effect of the substrate on the effective medium dielectric constant. In addition we found that the peak shift is determined by hot spots on the nanoparticle surface that are associated with less than 10% of the surface area.

By putting these results in perspective, the LSPR nanoparticle-based optical sensor can be optimized to produce varying responses to adsorbate molecules directly on their surfaces. This tunable sensitivity can be used to maximize the LSPR response of adsorbates, such as biomolecules and environmental contaminants, at the surface of nanoparticles. Because the long range distance dependence of nanoparticles varies with these same parameters,[1] to best optimize nanoparticle sensors, a balance between these parameters must be met.

Acknowledgment. We gratefully acknowledge financial support from the Nanoscale Science and Engineering Initiative of the National Science Foundation under NSF Award EEC-0118025. A.J.H. also acknowledges the American Chemical Society Division of Analytical Chemistry sponsored by Eastman Chemical and Dupont for fellowship support.

References and Notes

(1) Haes, A. J.; Zou, S.; Schatz, G. C.; Van Duyne, R. P. *J. Phys. Chem. B* **2004**, *108*, 109.

(2) Taton, T. A.; Lu, G.; Mirkin, C. A. *J. Am. Chem. Soc.* **2001**, *123*, 5164.

(3) Schultz, S.; Smith, D. R.; Mock, J. J.; Schultz, D. A. *Proc. Natl. Acad. Sci. U.S.A.* **2000**, *97*, 996.
(4) Taton, T. A.; Mirkin, C. A.; Letsinger, R. L. *Science* **2000**, *289*, 1757.
(5) Sonnichsen, C.; Franzl, T.; Wilk, T.; von Plessen, G.; Feldmann, J.; Wilson, O.; Mulvaney, P. *Phys. Rev. Lett.* **2002**, *88*, 077402/1.
(6) Sonnichsen, C.; Geier, S.; Hecker, N. E.; von Plessen, G.; Feldmann, J.; Ditlbacher, H.; Lamprecht, B.; Krenn, J. R.; Aussenegg, F. R.; Chan, V. Z.-H.; Spatz, J. P.; Moller, M. *Appl. Phys. Lett.* **2000**, *77*, 2949.
(7) Yguerabide, J.; Yguerabide, E. E. *Anal. Biochem.* **1998**, *262*, 157.
(8) Yguerabide, J.; Yguerabide, E. E. *Anal. Biochem.* **1998**, *262*, 137.
(9) Bao, P.; Frutos, A. G.; Greef, C.; Lahiri, J.; Muller, U.; Peterson, T. C.; Wardern, L.; Xie, X. *Anal. Chem.* **2002**, *74*, 1792.
(10) Connolly, S.; Cobbe, S.; Fitzmaurice, D. *J. Phys. Chem. B* **2001**, *105*, 2222.
(11) Connolly, S.; Rao, S. N.; Fitzmaurice, D. *J. Phys. Chem. B* **2000**, *104*, 4765.
(12) Elghanian, R.; Storhoff, J. J.; Mucic, R. C.; Letsinger, R. L.; Mirkin, C. A. *Science* **1997**, *227*, 1078.
(13) Mirkin, C. A.; Letsinger, R. L.; Mucic, R. C.; Storhoff, J. J. *Nature* **1996**, *382*, 607.
(14) Storhoff, J. J.; Elghanian, R.; Mucic, R. C.; Mirkin, C. A.; Letsinger, R. L. *J. Am. Chem. Soc.* **1998**, *120*, 1959.
(15) Storhoff, J. J.; Lazarides, A. A.; Mucic, R. C.; Mirkin, C. A.; Letsinger, R. L.; Schatz, G. C. *J. Am. Chem. Soc.* **2000**, *122*, 4640.
(16) Kreibig, U.; Gartz, M.; Hilger, A. *Ber. Bunsen-Ges.* **1997**, *101*, 1593.
(17) Kreibig, U.; Vollmer, M. *Cluster Materials*; Springer-Verlag: Heidelberg, Germany, 1995; Vol. 25.
(18) Malinsky, M. D.; Kelly, K. L.; Schatz, G. C.; Van Duyne, R. P. *J. Am. Chem. Soc.* **2001**, *123*, 1471.
(19) Linnert, T.; Mulvaney, P.; Henglein, A. *J. Phys. Chem.* **1993**, *97*, 679.
(20) Hilger, A.; Cuppers, N.; Tenfelde, M.; Kreibig, U. *Eur. Phys. J. D* **2000**, *10*, 115.
(21) Henglein, A.; Meisel, D. *J. Phys. Chem. B* **1998**, *102*, 8364.
(22) Nath, N.; Chilkoti, A. *Anal. Chem.* **2002**, *74*, 504.
(23) Eck, D.; Helm, C. A.; Wagner, N. J.; Vaynberg, K. A. *Langmuir* **2001**, *17*, 957.
(24) Okamoto, T.; Yamaguchi, I.; Kobayashi, T. *Opt. Lett.* **2000**, *25*, 372.
(25) Himmelhaus, M.; Takei, H. *Sens. Actuators B* **2000**, *B63*, 24.
(26) Takei, H. *Proc. SPIE-Int. Soc. Opt. Eng.* **1998**, *3515*, 278.
(27) Haes, A. J.; Van Duyne, R. P. *J. Am. Chem. Soc.* **2002**, *124*, 10596
(28) Haes, A. J.; Van Duyne, R. P. *Mater. Res. Soc. Symp. Proc.* **2002**, *723*, O3.1.1.
(29) Riboh, J. C.; Haes, A. J.; McFarland, A. D.; Yonzon, C. R.; Van Duyne, R. P. *J. Phys. Chem. B* **2003**, *107*, 1772.
(30) Cao, Y. W.; Jin, R. C.; Mirkin, C. A. *Science* **2002**, *297*, 1536.
(31) Hirsch, L. R.; Jackson, J. B.; Lee, A.; Halas, N. J.; West, J. L. *Anal. Chem.* **2003**, *75*, 2377.
(32) McFarland, A. D.; Van Duyne, R. P. *Nano Lett.* **2003**, *3*, 1057.
(33) El-Sayed, M. A. *Acc. Chem. Res.* **2001**, *34*, 257.
(34) Link, S.; El-Sayed, M. A. *J. Phys. Chem. B* **1999**, *103*, 8410.
(35) Jensen, T. R.; Malinsky, M. D.; Haynes, C. L.; Van Duyne, R. P. *J. Phys. Chem. B* **2000**, *104*, 10549.
(36) Michaels, A. M.; Nirmal, M.; Brus, L. E. *J. Am. Chem. Soc.* **1999**, *121*, 9932.
(37) Schatz, G. C.; Van Duyne, R. P. *Electromagnetic Mechanism of Surface-Enhanced Spectroscopy*; Wiley: New York, 2002; Vol. 1.
(38) Kelly, K. L.; Coronado, E.; Zhao, L.; Schatz, G. C. *J. Phys. Chem. B* **2003**, *107*, 668.
(39) Haynes, C. L.; Van Duyne, R. P. *J. Phys. Chem. B* **2001**, *105*, 5599.
(40) Mulvaney, P. *MRS Bull.* **2001**, *26*, 1009.
(41) Mulvaney, P. *Langmuir* **1996**, *12*, 788.
(42) Kreibig, U.; Gartz, M.; Hilger, A.; Hovel, H. Optical investigations of surfaces and interfaces of metal clusters. In *Advances in Metal and Semiconductor Clusters*; Duncan, M. A., Ed.; JAI Press Inc.: Stamford, CT, 1998; Vol. 4, p 345.
(43) Kreibig, U. Optics of nanosized metals. In *Handbook of Optical Properties*; Hummel, R. E., Wissmann, P., Eds.; CRC Press: Boca Raton, FL, 1997; Vol. II, p 145.
(44) Jensen, T. R.; Kelly, K. L.; Lazarides, A.; Schatz, G. C. *J. Cluster Sci.* **1999**, *10*, 295.
(45) Haynes, C. L.; McFarland, A. D.; Zhao, L.; Van Duyne, R. P.; Schatz, G. C.; Gunnarsson, L.; Prikulis, J.; Kasemo, B.; Käll, M. *J. Phys. Chem. B* **2003**, *107*, 7337.
(46) Hulteen, J. C.; Van Duyne, R. P. *J. Vac. Sci. Technol. A* **1995**, *13*, 1553.
(47) Jensen, T. R.; Schatz, G. C.; Van Duyne, R. P. *J. Phys. Chem. B* **1999**, *103*, 2394.
(48) Zeman, E. J.; Schatz, G. C. *J. Phys. Chem.* **1987**, *91*, 634.
(49) Walczak, M. M.; Chung, C.; Stole, S. M.; Widrig, C. A.; Porter, M. D. *J. Am. Chem. Soc.* **1991**, *113*, 2370.
(50) Acker, W. P.; Schlicht, B.; Chang, R. K.; Barber, P. W. *Opt. Lett.* **1987**, *12*, 465.
(51) Li, J.; Liang, K. S.; Camillone, N. I.; Leung, T. Y. B.; Scoles, G. *J. Chem. Phys.* **1995**, *102*, 5012.
(52) Porter, M. D.; Bright, T. B.; Allara, D. L.; Chidsey, C. E. D. *J. Am. Chem. Soc.* **1987**, *109*, 3559.
(53) Geer, R. E.; Stenger, D. A.; Chen, M. S.; Calvert, J. M.; Shashidhar, R.; Jeong, Y. H.; Pershan, P. S. *Langmuir* **1994**, *10*, 1171.
(54) Wasserman, S. R.; Whitesides, G. M.; Tidswell, I. M.; Ocko, B. M.; Pershan, P. S.; Axe, J. D. *J. Am. Chem. Soc.* **1989**, *111*, 5852.
(55) Peterlinz, K. P.; Georgiadis, R. *Opt. Commun.* **1996**, *130*, 260.
(56) Draine, B. T.; Flatau, P. J. *J. Opt. Soc. Am. A* **1994**, *11*, 1491.
(57) Lynch, D. W.; Hunter, W. R. In *Handbook of Optical Constants of Solids*; Palik, E. D., Ed.; Academic Press: New York, 1985; p 350.